Ab Initio Prediction of Adsorption Isotherms for Small Molecules in Metal–Organic Frameworks

Arpan Kundu,[†] GiovanniMaria Piccini,[†] Kaido Sillar,[†,‡] and Joachim Sauer[*,†]

[†]Institut für Chemie, Humboldt-Universität zu Berlin, Unter den Linden 6, 10099 Berlin, Germany
[‡]Institute of Chemistry, University of Tartu, Ravila 14 a, 50411 Tartu, Estonia

S *Supporting Information*

ABSTRACT: For CO and N_2 on Mg^{2+} sites of the metal–organic framework CPO-27-Mg (Mg-MOF-74), ab initio calculations of Gibbs free energies of adsorption have been performed. Combined with the Bragg-Williams/Langmuir model and taking into account the experimental site availability (76.5%), we obtained adsorption isotherms in close agreement with those in experiment. The remaining deviations in the Gibbs free energy (about 1 kJ/mol) are significantly smaller than the "chemical accuracy" limit of about 4 kJ/mol. The presented approach uses (i) a DFT dispersion method (PBE+D2) to optimize the structure and to calculate *anharmonic frequencies* for vibrational partition functions and (ii) a "hybrid MP2:(PBE+D2)+ΔCCSD(T)" method to determine electronic energies. With the achieved accuracy (estimated uncertainty ±1.4 kJ/mol), the ab initio energies become useful benchmarks for assessing different DFT + dispersion methods (PBE+D2, B3LYP+D*, and vdW-D2), whereas the ab initio heats, entropies, and Gibbs free energies of adsorption are used to assess the reliability of experimental values derived from fitting isotherms or from variable-temperature IR studies.
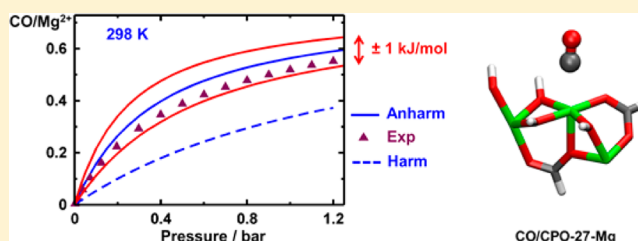
1. INTRODUCTION

There is much and growing interest in the storage and separation of small energy-related molecules in nanoporous materials such as metal–organic frameworks (MOFs) and zeolites. The key descriptor for the design of new materials with improved properties is the adsorption isotherm, $n = f_T(P)$, which determines the gas amount n adsorbed at a given temperature T as a function of the gas pressure P. Its prediction requires the calculation of free energies of adsorption with only the structure as input. Since simulation cells on the order of 1000 atoms are required, this is a computationally very challenging task. Approximate methods have been proposed that make the screening of a large number of structures possible.[1,2] They are based on computationally efficient grand canonical Monte Carlo (GCMC) simulations and use simple force fields validated on experiments.[1]

To test such approximate methods and as a foundation for their further development, a set of benchmark systems is necessary for which convergence has been achieved within chemical accuracy limits (4 kJ/mol) between accurate results from ab initio calculations and accurate experimental data for well-characterized surfaces. For molecules in the gas phase, the availability of benchmark sets has facilitated the development of computational quantum chemical models very much[3,4] and still does.[5] It is our aim to establish such benchmark sets for molecule–surface interactions. For adsorption on flat surfaces (CO on MgO(001))[6] and in zeolites (small alkanes in H-chabazite),[7] this has already been achieved.

Here, we extend this data set to the adsorption of CO and N_2 on five-fold-coordinated Mg^{2+} sites in a metal–organic framework (MOF).[8] We will show that our computational ab initio approach yields Gibbs free energies of adsorption within 1 kJ/mol of experimental results.[9,10] We will further show that enthalpies (and entropies) derived from experimental isotherm data[9] or from variable-temperature infrared (VTIR) experiments[11,12] are less suitable to assess computational results than the isotherms themselves or the free energies obtained from them with Langmuir fits.

State-of-the-art methodology to calculate ab initio Gibbs free energies for adsorption complexes is (i) use of density functional theory (DFT) with some account of dispersion (DFT-D) for obtaining the electronic energies (for MOFs, see, ref 13) in combination with (ii) use of harmonic vibrational frequencies for obtaining enthalpies and entropies at finite temperatures from molecular statistics.[14–20] Here, we use methodology that improves with both steps. (i) For improved energies, we apply a hybrid method that combines DFT for the full periodic system with wave-function-type electron correlation methods for the adsorption site.[21,22] (ii) For improved vibrational contributions to entropies and enthalpies, we use anharmonic vibrational frequencies instead of harmonic ones. We avoid the prohibitively large computational effort (exponential scaling with system size) of a full anharmonicity calculation by solving one-dimensional Schrödinger equations
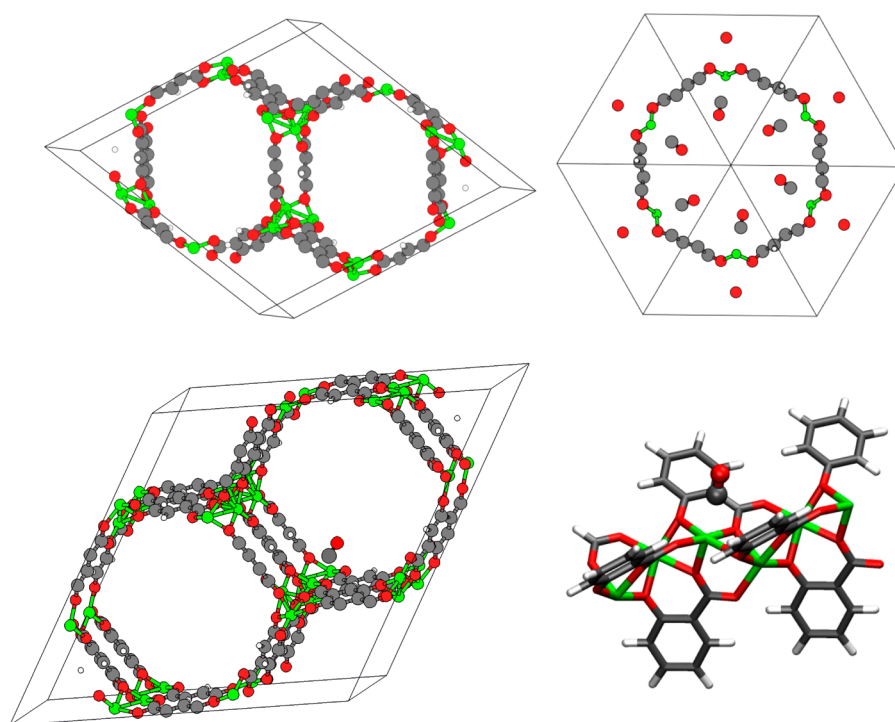
Figure 1. CPO-27-Mg. Top: Conventional unit cell (left) and primitive unit cell with six CO (C-down) molecules at Mg^{2+} sites (right). Bottom: Conventional unit cell doubled along the *c*-direction (2xcuc) with only one CO molecule (left) and **6B** cluster model adopted for MP2 calculations. Color code: green, magnesium; red, oxygen; gray, carbon; white, hydrogen.

for each vibrational (normal) mode separately.[23,24] For adsorption of small alkanes in zeolites,[7] this approach has yielded enthalpies and Gibbs free energies within 3 kJ/mol and rate constants for the methylation of alkenes in zeolites within less than 1 order of magnitude of the experimental values.[25]

Very recently, an alternative approach to include anharmonicity for molecule−surface interactions (ethanol in zeolite H-ZSM-5) has been proposed.[26] Molecular dynamics (MD) is used to get the vibrational density of states, from which the partition function is calculated. The MD run can be much shorter compared to a direct free energy simulation.

We examine the adsorption of CO and N_2 on CPO-27-Mg,[8] see refs 9,12,27−29 for previous quantum chemical studies. The CPO-27 frameworks, also named MOF-74,[30] are isostructural compounds in which divalent metal ions (M^{2+}) are connected by 2,5-dioxido-1,4-benzenedicarboxylate ($dobdc^{4-}$) linkers. The resulting three-dimensional $M_2(dobdc)$ framework has a trigonal structure with one-dimensional hexagonal pores (Figure 1). The $dobdc^{4-}$ linkers form the wall of the channel, whereas the vertices of the pore walls contain five-fold-coordinated Mg^{2+} ions which resemble the Mg^{2+} sites on the much simpler MgO(001) terraces. In CPO-27-Mg, there are additional interactions with the surrounding linkers, which makes the binding of CO to the five-fold-coordinated Mg^{2+} sites almost twice as strong (43 kJ/mol; see below) as the binding to the corresponding terraces sites on the MgO(001) surface (21 kJ/mol).[6]

2. METHODS AND MODELS

2.1. Adsorption Isotherms and Gibbs Free Energies.
Ab initio calculations of Gibbs free energies of adsorption, ΔG, require (i) a quantum chemical method for calculating points on the potential energy surface (PES) and (ii) a statistical method for sampling the PES. One option for (ii) is explicit sampling by Monte Carlo (MC) or

MD. This means that nuclei are treated classically, and this implies the need to evaluate the electronic energy for millions of configurations "on the fly".[31] This is only affordable if reliable force fields are available. For molecule−surface interactions, in general, and for MOFs, in particular,[13] this is rarely the case. For small molecules in MOFs, MC simulations have been reported that use non-empirical force fields but assume rigid pore structures.[32,33] Very few attempts have been made to sample the PES obtained from DFT directly by MC or MD, such as for small alkane molecules in zeolites.[34,35] Our approach[7,36,37] relies on ab initio Gibbs free energies (equilibrium constants K) for adsorption complexes at individual surface sites and makes use of model isotherms, such as the Langmuir isotherm, to include the configurational entropy resulting from the distribution of adsorbed gas molecules over the sites. The free energies for an individual site are calculated from vibrational partition functions, q_{vib}, which correspond to an analytical sampling for a Taylor expansion of the full PES around a local minimum.

With the Bragg-Williams (mean-field) approximation for lateral interactions,[37,38] $E_{lat}(\theta)$, the equilibrium constant of adsorption *at individual sites* at temperature T, $K_{BW}(\theta)$, is obtained from the Gibbs free adsorption energy, ΔG (R is the gas constant, and ΔH and ΔS are the adsorption enthalpy and entropy, respectively)

$$K_{BW}(\theta) = \exp\left(\frac{-\Delta G}{RT}\right) = \exp\frac{\Delta S}{R}\exp\left(\frac{-\Delta H}{RT}\right) \quad (1)$$

Taking the distribution of adsorbed molecules over the available number of sites into account (configurational entropy), the surface coverage, θ, as a function of P, is given by the Langmuir isotherm. With the Bragg-Williams approximation for lateral interactions, this yields

$$\theta = \frac{K_{BW}(\theta)P}{1 + K_{BW}(\theta)P} \quad (2)$$

The ΔG value for individual adsorption sites is obtained with the approach defined by steps (i) and (ii) in the Introduction. It is composed of the enthalpy, ΔH, and entropy of adsorption, ΔS

$$\Delta G = \Delta H - T\Delta S \qquad (3)$$

The adsorption enthalpy is calculated from

$$\Delta H = \Delta E^{\text{final}} + \Delta E^{\text{ZPV}} + \Delta E^{\text{thermal}} - RT \qquad (4)$$

where ΔE^{final}, ΔE^{ZPV}, and $\Delta E^{\text{thermal}}$ are the changes on adsorption of the electronic energy, the zero-point vibrational energy (ZPV), and the thermal energy, respectively.

With the pre-exponential defined by the partition functions q for the loaded MOF (q_a), the unloaded MOF (q_{MOF}), and the gas molecule (q_M), the equilibrium constant becomes

$$K_{\text{BW}}(\theta) = \frac{q_a}{q_{\text{MOF}}q_M}\exp\left(\frac{-\Delta E^{\text{final}} - \Delta E^{\text{ZPV}} - E_{\text{lat}}(\theta)}{RT}\right) \qquad (5)$$

Calculating Bragg-Williams adsorption isotherms, eq 2 with inclusion of lateral interactions (eq 5) requires an iterative process because the mean lateral interaction depends on the coverage θ. As an initial guess, θ is calculated for $E_{\text{lat}} = 0$, that is, $\theta = 0$.

The lateral interaction energy is calculated from average pair interaction energies, E_{pair}, as a function of the total coverage

$$E_{\text{lat}}(\theta) = \frac{1}{2}N\theta E_{\text{pair}} \qquad (6)$$

N is the number of adsorbate neighbors exerting the lateral interaction. $N\theta$ is the number of laterally interacting neighbors experienced by an adsorbate molecule on average.

2.2. Quantum Chemical Calculations of Adsorption Energies. We apply a hybrid high-level:low-level quantum method that combines DFT for the full periodic system with second-order Møller–Plesset perturbation theory (MP2) for the reaction site.[21,22] To check if MP2 is accurate enough, we calculate coupled cluster (CC) corrections with single, double, and perturbatively treated triple substitutions (CCSD(T)) for sufficiently small models of the reaction site.[22]

The hybrid MP2:PBE+D2 adsorption energy, $\Delta E^{\text{MP2:PBE+D2}}$, is defined by the subtraction scheme

$$\Delta E^{\text{MP2:PBE+D2}} = \Delta E^{\text{PBE+D2,pbc}}(S) + \Delta E^{\text{MP2}}(C) - \Delta E^{\text{PBE+D2}}(C) \qquad (7)$$

which requires three calculations for each structure: the PBE+D2 energy for the full periodic structure S (periodic boundary conditions), $\Delta E^{\text{PBE+D2,pbc}}(S)$, and MP2 and PBE+D2 energies for the finite-sized cluster model C, $\Delta E^{\text{MP2}}(C)$ and $\Delta E^{\text{PBE+D2}}(C)$, respectively.

There are two ways to look at the hybrid scheme. A high-level (MP2) correction, Δ_{HL}, is added to the DFT+D energy of the full periodic system, or a long-range (DFT+D) correction, Δ_{LR}, is added to the high-level (MP2) energy of the cluster:

$$\Delta E^{\text{MP2:PBE+D2}} = \Delta E^{\text{PBE+D2,pbc}}(S) + \Delta_{\text{HL}}(C)$$
$$= \Delta E^{\text{MP2}}(C) + \Delta_{\text{LR}}(S, C) \qquad (8)$$

with

$$\Delta_{\text{HL}}(C) = \Delta E^{\text{MP2}}(C) - \Delta E^{\text{PBE+D2}}(C) \qquad (9)$$

and

$$\Delta_{\text{LR}}(S, C) = \Delta E^{\text{PBE+D2,pbc}}(S) - \Delta E^{\text{PBE+D2}}(C) \qquad (10)$$

Higher-order correlation effects are included using CCSD(T), which was only affordable for small cluster models C′ shown in Figure 2 (C′ = **M1**, **MA**, **MB**). The coupled cluster correction is defined as

$$\Delta_{\text{CCSD(T)}} = \Delta E^{\text{CCSD(T)}}(C') - \Delta E^{\text{MP2}}(C') \qquad (11)$$

The final adsorption energy is the sum of hybrid MP2 adsorption energy and the coupled cluster correction at the PBE+D2 optimized structure:

$$\Delta E^{\text{final}} = \Delta E^{\text{MP2:PBE+D2}} + \Delta_{\text{CCSD(T)}} \qquad (12)$$

2.3. DFT+D Calculations on Periodic Models. The primitive unit cell (puc) of CPO-27 is composed of six Mg^{2+} ions and three dobdc linkers, corresponding to three Mg_2(dobdc) formula units, whereas the conventional unit cell (cuc) consists of nine formula units (see Table 1).[8] Previous DFT calculations have been performed for six

Table 1. Composition and Lattice Parameters (pm or degree) of Different Periodic Models

	puc[a]	2xcuc[b]
Mg^{2+}	6	36
dobdc[4−]	3	18
$a = b$	1522.2	2608.9
c	1522.2	1375.8
$\alpha = \beta$	117.8	90.0
γ	117.8	120.0

[a]See Figure 1, top right. [b]See Supporting Information Figure S1.

adsorbate molecules per six Mg^{2+} ions in the puc.[9,12,27−29] Here, we also perform DFT+D calculations for this model to obtain vibrational frequencies as input for the ZPV energies and partition functions. Both cell parameters and fractional coordinates were optimized.

To determine the adsorption energy, first the conventional unit cell of the framework (see Figure 1, top left) was loaded with only one adsorbate molecule (one adsorbate per 18 Mg^{2+} ions), and cell parameters were optimized. Then the cell was doubled along the c direction (2xcuc), but only one adsorbate molecule (one per 36 Mg^{2+} ions) was accommodated inside the MOF framework (Figure 1, bottom left). This was done to exclude lateral interactions which were calculated separately. The ion positions were then reoptimized, keeping the cell parameters fixed. From these optimized structures, cluster models were cut out. Table 1 shows the cell parameters obtained.

The DFT calculations employed the Perdew−Burke−Ernzerhof (PBE) functional[39,40] with Grimme's semiempirical "D2" dispersion term[41] and were performed with the Vienna ab initio simulation package (VASP)[42,43] modified to include dispersion under periodic boundary conditions.[44] We do not use the original D2 Mg parameters for Mg^{2+} but follow the recommendation of Tosoni and Sauer[45] and adopt the original Ne parameters. Periodic boundary conditions were applied and the calculations performed for a single k-vector (0.5, 0.5, 0.5) in the Brillouin zone. A plane wave basis set with an 800 eV kinetic energy cutoff was used for the valence electrons (including the 2p electrons of Mg^{2+} ions), whereas core electrons were described by the projector-augmented wave method.

2.4. MP2 and CCSD(T) Calculations on Cluster Models. Figures 1 (bottom right) and 2 show the finite-sized cluster models
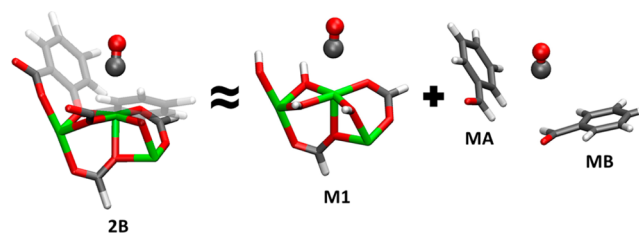

Figure 2. **M1**, **MA**, and **MB** models adopted for CCSD(T) calculations and their relation to the **2B** model.

adopted for MP2 and CCSD(T) calculations, respectively. The CO molecule is shown in ball-and-stick representation. For MP2 calculations, a model was cut out from the 2xcuc cell which features six Mg^{2+} ions and six benzene rings (Figure 1, bottom right) and which we will call **6B**. For CCSD(T) calculations, a set of smaller models was adopted. Apart from the adsorbed molecule (CO, N_2), the **2B** cluster model (Figure 2) contains two formate anions and two 2-oxido-benzoate dianions, but it is too large for CCSD(T) calculations.

Therefore, the "subclusters" **M1**, **MA**, and **MB** (Figure 2) are used to calculate the interaction of the adsorbate with the Mg^{2+} sites. To avoid double counting, the cuts were made such that any "real" atom was part of only one of the models, **M1** or **MA/MB** (see Supporting Information, Figure S2). The **M1** model contains three Mg^{2+} ions, two formate anions, and four hydroxide anions. Each of the **MA** and **MB** models contains a single benzaldehyde unit.

MP2 and CCSD(T) calculations were performed using the ricc2 module[46] of Turbomole version 6.5.[47] Only valence shell electrons were correlated, with the 2p electrons of Mg^{2+} treated as a valence shell. The counterpoise (CP) correction scheme[48] was applied to correct for the basis set superposition error (BSSE). The BSSE-corrected adsorption energies calculated with Dunning's correlation-consistent aug-cc-pVxZ basis sets (with x = D,T)[49,50] were extrapolated to the complete basis set limit and are referred to as CBS(D,T) values. For the Hartree−Fock contribution of the energies, an exponential ansatz[51,52] was employed, whereas inverse power behavior[51,53] was assumed for the correlation contribution.

2.5. Partition Functions and Vibrational Energies. State-of-the-art calculations sample the potential surface for individual adsorption sites "analytically" by calculating partition functions from harmonic vibrational frequencies.[14−20] The main limitation of the harmonic oscillator model is that small vibrational frequencies make the largest contribution to the entropies (see ref 54 section 10.5.2) and that relatively small errors on these frequencies lead to large errors in the entropy term. This is particularly true for the hindered translations and rotations of adsorbed molecules on the surface. Sometimes, it is better to assume that the molecules are freely rotating on the surface (H_2 and CH_4 in MOFs),[36,37] or that free rotation and translation is preserved at least for some degrees of freedom (alkanes on MgO(001);[55] see refs 56 and 57 for recent extensions of this approach) than to describe such modes as harmonic vibrations. Also the (hindered) internal rotations of alkane require special treatment beyond the harmonic approximation.[17]

Here, we calculate normal modes and harmonic vibrational energies for the DFT-D potential energy surface only as a first step. We reduce the scaling of the $3N$-dimensional (N number of atoms) anharmonic vibrational problem from exponential to linear by solving $3N$ one-dimensional Schrödinger equations for each normal mode separately.[23,24] Since finite-sized distortions are needed to calculate the one-dimensional potentials, the rectilinear normal coordinates need to be represented in curvilinear internal coordinates.[7,24,58] For example, when rotating a molecule relative to the surface, this ensures that its bond distances and bond angles do not change. The calculated points were fitted with an anharmonic nth-order polynomial, and the $3N$ one-dimensional Schrödinger equations were solved variationally in a basis of harmonic oscillator functions.

For the partition functions in eq 5, all possible degrees of freedom (translation, rotation, and vibration) were taken into account for the gas, whereas only vibrational contributions were considered for solids. The partition function for each vibrational degree of freedom was expressed as a finite sum of m states:[59]

$$q_{vib} = \sum_{i=1}^{\infty} \exp\left(-\frac{\varepsilon_i}{k_B T}\right) \approx \sum_{i=1}^{m} \exp\left(-\frac{\varepsilon_i}{k_B T}\right) \tag{13}$$

The anharmonic vibrational energies, ε_i, which are given with respect to the vibrational ground level, were calculated following the computational protocol of Piccini and Sauer.[7,23,24] Details are provided in the Supporting Information.

3. RESULTS AND DISCUSSION

3.1. DFT+D Results. *3.1.1. Structures.* The PBE+D2 cell parameters obtained for the empty cuc of CPO-27-Mg ($a = b = 2608.9$ and $c = 687.9$ pm) are in good agreement with the available experimentally determined lattice constants, $a = b = 2589.2$,[60] 2591.1,[61] 2592.1,[62] and 2602 pm[63] and $c = 672.1$,[63] 686.2,[62] 686.9,[61] and 687.4 pm.[60] The $a = b$ and c values are 0.3−0.8 and 0.1−2.3%, respectively, larger than the exper-

imental values. A decrease of the cell volume by 1.4% is observed upon adsorption of a CO molecule on all Mg^{2+} sites, that is, $CO/Mg^{2+} = 1$ (18 CO/cuc = 6 CO/puc). The lattice constants a, b, and c change by −28.8, −33.4, and 8.5 pm, respectively. For N_2 loading, the cuc volume shrinks 0.4% only, and the a, b, and c parameters change by −11.5, −17.7, and 5.8 pm, respectively.

Figure 3 shows the local structures of the CO and N_2 adsorption complexes on the Mg^{2+} sites. Table 2 shows the
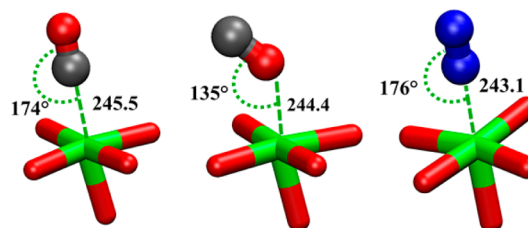

Figure 3. Adsorption complexes for Mg−CO (left), Mg−OC (middle), and Mg−N_2 (right). Bond distances (pm) and angles (degree) are reported for six adsorbate molecules/six Mg^{2+} ions (puc). Color code: green, magnesium; red, oxygen; gray, carbon; blue, nitrogen.

bond distances and angles. Both CO and N_2 bind to the Mg^{2+} ions almost linearly. CO can bind to the Mg^{2+} ion also with its "O" end (O-down),[64] but this is a less stable local minimum structure. For six CO (or N_2) molecules per six Mg^{2+} ions (puc), not all surface complexes have exactly the same bond distances and angles because we did not enforce symmetry constraints during the optimization.

For the O-down isomer, we obtain two different sets of structures, an almost linear one with Mg−O−C angles of about 169−172° and a bent one with Mg−O−C angles of 135° (Figure 3, middle), which are alternating in the primitive unit cell (Supporting Information, Figure S1).

For CO (C-down), our PBE+D2 adsorption structures are similar to the ones obtained with a van der Waals (vdW) density functional.[65] Compared to the previously reported B3LYP+D* structures,[12] our Mg−C distances are about 3 pm shorter but still 4−5 pm longer than the 241 pm obtained with neutron powder diffraction for CO on Mg-MOF-74 ($\theta = 0.75$).[9] The latter also yields a more bent structure (Mg−C−O angle = 167°). One should keep in mind, however, that DFT+D yields an r_e structure (bottom of the potential well), while neutron diffraction yields an average structure at the experimental temperature (10 K). In contrast, for the Mg−N distance in the Mg−N−N complex, the PBE+D2 distance is 1.5−1.9 pm longer than the B3LYP+D* distance.

3.1.2. Adsorption Energies. Most of previous computational studies[12,27,29,65] on CO/CPO-27-Mg and N_2/CPO-27-Mg have reported average adsorption energies per adsorbed molecules, defined as

$$\Delta E = (E(M_m \cdot MOF) - E(MOF) - mE(M))/m \tag{14}$$

with $m = 6$. This definition of the adsorption energy effectively includes lateral interactions between adsorbates. Table 2 shows such PBE+D2 results compared to previously obtained B3LYP+D* values for six molecules/six Mg^{2+} ions in puc.[12] For Mg−N_2, the differences are small, but for Mg-CO, PBE+D2 predicts 7 and 8 kJ/mol stronger binding than with the vdW-DF (−33.6 kJ/mol).[65] The latter also predicts a too stable Mg−OC (O-down) isomer (−31.3 kJ/mol) compared to PBE+D2.

Table 2. Bond Angles (degree), Mg−A Bond Distances, and A−B Bond Distance Changes on Adsorption (pm), as Well as Adsorption Energies Per Molecule, ΔE (kJ/mol)

complex	method	loading Θ (CO/Mg^{2+})	∠Mg−A−B	R(Mg−A)	ΔR(A−B)	$-\Delta E^{b}$
Mg−C−O	PBE+D2	1/36 (2xcuc)	177	244.8	−0.4^{c}	40.4 (13.6)
(C-down)	PBE+D2	1 (2xcuc//puc)				39.9 (16.0)
	PBE+D2	1 (puc)	174	245.5−245.9	−0.2^{c}	41.5 (16.0)
	B3LYP+D*^{a}	1 (puc)	178	248.6	−0.5^{d}	34.3 (18.1)
Mg−O−C	PBE+D2	1/36 (2xcuc)	137	240.4	+0.7	24.5 (15.5)
(O-down)	PBE+D2	1 (2xcuc//puc)				24.2 (15.4)
	PBE+D2	1 (puc)	135	244.4	+0.7	21.1 (15.4)
			169−172	242.5	+0.2	
Mg−N−N	PBE+D2	1/36 (2xcuc)	178	241.6	−0.2^{e}	29.3 (12.9)
	PBE+D2	1 (2xcuc//puc)				29.0 (14.5)
	PBE+D2	1 (puc)	176	243.1−243.4	−0.2^{e}	29.1 (14.5)
	B3LYP+D*^{a}	1 (puc)	175	241.5	−0.2^{f}	27.1 (19.0)

^{a}From ref 12. ^{b}Dispersion contribution in parentheses. ^{c}The gas phase C−O distance with PBE+D2 is 114.3 pm. ^{d}The gas phase C−O distance with B3LYP+D* is 112.7 pm. ^{e}The gas phase N−N distance with PBE+D2 is 111.3 pm. ^{f}The gas phase N−N distance with B3LYP+D* is 109.3 pm.

Table 3. Adsorption Energies (kJ/mol) Calculated with Different Methods on Periodic PBE+D2 Structures (One Adsorbate/36 Mg^{2+} Sites, 2xcuc)

methods	M−CO			M−OC			M−N$_2$		
	6B^{a}	pbc^{b}	Δ_{LR}^{c}	**6B**^{a}	pbc^{b}	Δ_{LR}^{c}	**6B**^{a}	pbc^{b}	Δ_{LR}^{c}
PBE//PBE+D2	−26.80	−26.80	0.00	−6.76	−9.09	−2.33	−16.44	−16.36	0.08
D2//PBE+D2	−13.67	−13.56	0.11	−15.67	−15.45	0.23	−13.07	−12.91	0.16
PBE+D2	−40.47	−40.36	0.11	−22.44	−24.54	−2.10	−29.50	−29.26	0.24
MP2/cbs//PBE+D2	−45.38			−25.43			−36.58		
Δ_{HL}^{d}	−4.91			−2.99			−7.08		
$\Delta E^{MP2:PBE+D e}$	−45.27			−27.53			−36.34		
ΔCCSD(T)/cbs	2.31			3.30			3.95		
final^{f}	−42.96			−24.23			−32.39		

^{a}**6B** cluster models; see Figure 1, bottom right. ^{b}Periodic boundary conditions; see Figure 1, bottom left. ^{c}Long-range correction (eq 10). ^{d}High-level correction (eq 9). ^{e}Hybrid MP2:PBE+D energy defined by eq 7. ^{f}See eq 12.

Table 2 also shows results for the same optimized puc structure, but six times replicated to yield a double conventional cell (2xcuc) with 36 adsorbed molecules per 36 Mg^{2+} ions. Since the number of plane waves and, hence, the basis set quality depend on the unit cell volume, the DFT results for the puc and the 2xcuc are not identical if the same kinetic energy cutoff (800 eV) is applied. The interaction energy changes by 1.6, 3.1, and 0.1 kJ/mol for Mg^{2+}−CO, Mg^{2+}−OC, and Mg^{2+}−NN, respectively, while the dispersion contribution that does not depend on the basis set remains constant.

In addition, Table 2 shows results for adsorption of a single molecule per 36 Mg^{2+} ions in a doubled conventional cell (2xcuc). The sums of these energies, −40.7 and −29.7 kJ/mol for Mg^{2+}−CO and Mg^{2+}−NN, respectively, and of the average lateral interaction energies (see Table 5 below) should be comparable to the adsorption energies for a loading of 36 molecules/36 Mg^{2+} ions in the 2xcuc cell, −39.9 and −29.0 kJ/mol for Mg^{2+}−CO and Mg^{2+}−NN, respectively. The differences of 0.8 and 0.7 kJ/mol, respectively, are due to different reference structures. The first has been optimized for $\theta = 1/36$ in 2xcuc, and the latter is the optimized puc structure for $\theta = 1$.

3.2. Hybrid MP2:DFT+D and CCSD(T) Energies. Whereas the vibrational partition functions are calculated for occupation of all Mg^{2+} sites (six adsorbate molecules/six Mg^{2+} sites, puc), the "final" energy that enters the calculation of the adsorption equilibrium constant (eq 5) is calculated for one molecule adsorbed in a double conventional cell (one adsorbate per 36 Mg^{2+} ions; see Figure 1, bottom left). This enables us to

cut **6B** clusters from both empty and loaded structures and, hence, calculate high-level energies including the effect of structure relaxation of the MOF.

Table 3 lists adsorption energies calculated with different methods on periodic PBE+D2 structures. All energies are single-point energies calculated at PBE+D2 optimized structures for one adsorbate molecule per 36 Mg^{2+} ions (2xcuc). The two configurations for CO adsorption, C-down and O-down, differ mainly in the PBE part of the PBE+D2 energy, while the dispersion contribution is similar. Hence, it is electrostatics that makes the Mg−CO configuration far more stable than the Mg−OC one. For the C-down configuration, the dispersion contribution is one-third of the total PBE+D2 adsorption energy, while for adsorption of N$_2$, dispersion and PBE are almost equally important.

The O-down configuration of CO remains unfavorable compared to the C-down configuration also after inclusion of the high-level corrections, and hence, it is not considered any further in this study.

The long-range corrections, that is, the difference between the PBE+D2 adsorption energies for the periodic model and the **6B** cluster model, are very small, for both the PBE and the dispersion part. This shows that the **6B** models are well-suited for MP2 calculations. Only for the O-down configuration, the long-range correction of the PBE contribution is about 25% of the periodic result but still less than 10% of the total PBE+D2 energy.

Table 4. Average Center of Mass Distance R (pm) and Average Interaction Energy (kJ/mol) of Two Molecules at Adjacent Adsorption Sites (Standard Deviation of the Set of Six Dimers Is Given in Parentheses)

		ΔE		ΔE, CBS(D,T)
system	R	PBE+D2	MP2	CCSD(T)
Mg−CO	492.5 (3.3)	−0.41 (0.022)	−0.56 (0.023)	−0.34 (0.016)
Mg−N$_2$	493.6 (0.9)	−0.42 (0.006)	−0.44 (0.006)	−0.35 (0.005)

Table 5. Comparison of Adsorption Energies (kJ/mol) and Molecule-Surface Distances (pm) Obtained with Different DFT-D Methods with the Final Estimate Based on the Hybrid Result (eq 15)

	R_{Mg-C}	CO[a]	R_{Mg-N}	N$_2$[a]
MP2:(PBE+D2)+$\Delta_{CCSD(T)}$	245[b]	−43.3 ± 1.8	242[b]	−32.7 ± 1.5
PBE+D2	246	−41.5 (1.8)	243	−29.1 (3.6)
vdW-DF2[e]	260	−38.8 (4.5)	251	−31.4 (1.3)
B3LYP+D*[c]	249	−34.3 (9.0)	242	−27.1 (5.6)
vdW-DF[d]		−33.6 (9.7)		

[a]Numbers in parentheses are difference to the final estimate. [b]One adsorbate molecule per 36 Mg^{2+} ions (2xcuc). [c]From ref 12. [d]From ref 65. [e]From ref 29.

Table 6. Thermodynamic Functions (kJ/mol) Calculated at 298 K Using Different Methods of Frequency Calculation for the PBE+D2 Potential Energy Surface (Contributions of Change in ZPV and Thermal (T) Energies Are Also Shown)

method	ΔE_{el}	ΔE_{ZPV}	ΔE_T	ΔH[a]	$-T\Delta S$	ΔG[a]
			M−CO/CPO-27-Mg			
harmonic[b]	−38.75	3.43	3.29	−34.51		
harmonic[c]	−34.3	3.5	0.7	−30.0	33.1	3.1
harmonic[d]	−42.96[e]	4.09	2.63	−38.71	38.68	−0.03
harmonic[f]	−42.96[e]	4.51	2.31	−38.62	40.54	1.93
anharmonic[f]	−42.96[e]	3.94	2.54	−38.95	37.84	−1.11
			M−N$_2$/CPO-27-Mg			
harmonic[b]	−31.42	2.72	3.65	−27.54		
harmonic[c]	−27.1	2.8				
harmonic[d]	−32.39[e]	2.94	3.58	−28.35	31.50	3.15
harmonic[f]	−32.39[e]	3.04	3.46	−28.37	33.05	4.68
anharmonic[f]	−32.39[e]	2.77	3.23	−28.87	31.82	2.94

[a]Contribution of $RT = -2.48$ kJ/mol. [b]Rigid MOF structure; only molecule−MOF vibrations included.[29] [c]Cartesian displacement.[12] [d]Standard approach as implemented in VASP. [e]Lateral interactions not included. [f]Numerical Hessian calculated by symmetric displacement along normal modes and one-dimensional fitting.[24]

Our hybrid MP2:PBE+D2 result for CO can be compared with the previous hybrid result based on B3LYP+D* for the DFT+D part, −45.4 kJ/mol.[27] In that study, the DFT-D interaction energy had been defined as the energy for removing one CO molecule from the fully loaded MOF without any structural change. Applying the same definition to the present study, we get −45.8 kJ/mol (see Supporting Information for details). Although different density functionals have been used, the final MP2:DFT-D hybrid energies differ by 0.4 kJ/mol only, which demonstrates the power of the hybrid scheme.

The differences between the coupled cluster, CCSD(T), and MP2 results in Table 3 (ΔCCSD(T)/cbs) are obtained from CCSD(T) and MP2 calculations for the **M1**, **MA**, and **MB** models shown in Figure 2; for details, see Table S2 of the Supporting Information. The benzene rings (**MA** and **MB** models) make repulsive contributions to the $\Delta_{CCSD(T)}$ values, in accord with well-known tendency of MP2 to overestimate binding energies of nonbonded interactions with conjugated π-systems.[66,67] The previous hybrid MP2:B3LYP+D* study[27] considered the **M1** model only, for which a CCSD(T)−MP2 difference of −0.2 kJ/mol was obtained for the M−CO adsorption complex. The Supporting Information also provides

an estimate of the uncertainty of the CCSD(T)−MP2 differences in Table 3, which is ±0.8 kJ/mol.

Lateral interaction energies are calculated as CCSD(T)/CBS(D,T) gas-phase dimerization energies of adsorbate molecules, which are shown in Table 4. The dimer structures were chosen from a puc (optimized at PBE+D2 level) with six adsorbate molecules and six Mg^{2+} ions. Considering only nearest neighbors, a set of six different dimers can be identified for six non-equivalent molecules, and their average is listed in Table 4.

3.3. Electronic Adsorption Energies. With the final estimate for isolated adsorbed molecules, eqs 8 and 12, the total electronic adsorption energy can be expressed as

$$\Delta E_{el} = \Delta E^{MP2} + \Delta_{LR} + E_{pair} + \Delta_{CCSD(T)} \qquad (15)$$

which reads for CO (in kJ/mol)

$$-43.3 = -45.4 + 0.1 - 0.3 + 2.3$$

and for N$_2$ (in kJ/mol)

$$-32.7 = -36.6 + 0.2 - 0.3 + 4.0$$

This shows that the lion's share of the electronic energy is obtained at the MP2 level for the **6B** cluster model. Our

complete basis set extrapolation is based on triple/double-ζ results. Previous studies on CO/MgO(001) show that using larger basis sets for extrapolation may increase the binding by not more than 0.2 kJ/mol (more negative number).[6]

Together with contributions from using different DFT-D reference structures (0.4 kJ/mol; see section 3.2), and adopting smaller models (**M1 + MA + MB**) for calculating $\Delta_{CCSD(T)}$ (0.8 kJ/mol; see Supporting Information), this yields ± 1.4 kJ/mol as our estimate for the uncertainty of the final electronic energies.

Compared to the final estimate (eq 15), PBE+D2 yields 1.8 and 3.6 kJ/mol weaker binding for CO and N$_2$, respectively (Table 5). For the vdW-D2 functional, the differences are of similar magnitude, while they are about twice as large (9.0 and 5.6 kJ/mol) for the B3LYP+D* functional.

3.4. Enthalpies, Entropies, and Gibbs Free Energies of Adsorption.

Table 6 shows thermodynamic functions obtained with different methods of frequency calculations. There are two sets of harmonic frequencies. Those obtained with the VASP code that are calculated from Cartesian displacements and suffer from numerical instabilities, in particular, for low-frequency modes. A conceptually better approach, denoted here as "**Harm**", is to make symmetric displacements along normal modes in a curvilinear fashion when calculating numerical harmonic frequencies.[24] Anharmonic frequencies obtained as described in section 2.4 will be abbreviated here as "**Anharm**".

At 298 K, the differences between **Anharm** and **Harm** results are small for enthalpies (below 0.5 kJ/mol) but larger for the entropy term $T\Delta S$ (1.7 and 1.2 kJ/mol for CO and N$_2$, respectively), yielding changes of -3.0 and -1.7 kJ/mol, respectively, for the Gibbs free energies. Although this may even change the sign of ΔG, the effect of anharmonicity is much smaller than that observed before for small alkane molecules in zeolites.[7] Due to some error cancellation, harmonic frequencies calculated with the VASP protocol (Cartesian displacements of 15 pm) yield Gibbs free energies of adsorption that are closer to the **Anharm** results than our **Harm** results.

3.5. Comparison with Experiment. 3.5.1. Adsorption Isotherms.

Figure 4 shows our calculated Bragg-Williams adsorption isotherms for CO and N$_2$ (eqs 2 and 5) compared to experiment. They use the energies and thermodynamic functions given in Table 6. The saturation coverage, N_{sat}, obtained from the Langmuir fit of the experimental adsorption isotherms does not agree with the coverage $N = 8.24$ mmol/g obtained for an ideal structure in which all Mg^{2+} sites are occupied. This indicates that, due to sample imperfections, not all sites of the ideal structure are available. Therefore, we calculated the percentage of experimentally available sites, N_{sat}/N, from the experimental isotherms. The N$_2$ isotherms[10] for 293 and 313 K yield somewhat different values, 83.3 and 69.4%, respectively, but their average (76.4%) is very close to the value obtained from the CO isotherms[9] for 298 and 318 K (76.5%). This is expected because the same sample/synthesis procedure is used. The values we obtain here (76.5%) are also very close to the value obtained for CH$_4$ adsorption on CPO-27-Mg (78%).[37] We scale all calculated isotherms with 76.5%.

Figure 4 shows close agreement between the anharmonic calculations (solid lines) and the isotherms measured for CO (298 K, ref 9) and N$_2$ (293 K, ref 10) on CPO-27-Mg (triangles). The corresponding isotherms for CO at 318 K and for N$_2$ at 313 K are shown in the Supporting Information. Solid
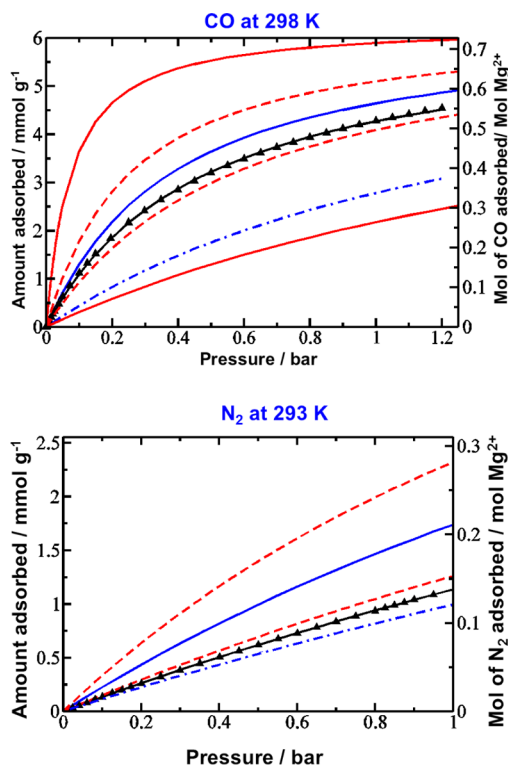

Figure 4. Calculated Bragg-Williams isotherms (scaled with experimental availability of sites, −76.5%) for CO/CPO-27-Mg at 298 K (top, blue) and N$_2$/CPO-27-Mg at 293 K (bottom, blue) compared to experiment[9,10] (triangles). Blue solid and dash-dotted lines are isotherms calculated from "anharmonic" and "harmonic" Gibbs free energies, respectively. Black solid lines represent the Langmuir fit of experimental data points.[9,10] Red solid and dashed lines represent the ± 4 kJ/mol (chemical accuracy) and ± 1 kJ/mol error bars, respectively, of Gibbs free energies.

and broken red lines represent ± 4 and ± 1 kJ/mol error bars of the Gibbs free energies from which the isotherms are calculated. The usual definition of "chemical accuracy" with 4 kJ/mol still means that the predicted adsorbed amount for a given pressure and temperature may be in error by a factor of 2. Figure 4 shows that the Gibbs free energies we calculated from anharmonic vibrational frequencies and ab initio energies obtained with our hybrid MP2:(PBE+D2)+ΔCCSD(T) approach even touch the accuracy level of ± 1 kJ/mol.

For CO, the harmonic calculations show deviations from the observed isotherms much larger than those of the anharmonic ones, whereas for N$_2$, the deviations of the harmonic and anharmonic approach are both small but with opposite sign. Given the small absolute deviations within the 1 kJ/mol range for both and the finite accuracy of the experimental isotherms, in particular, low loadings are observed with N$_2$. The slightly better agreement for the harmonic results does not mean that this is a better approximation; it rather reflects the fact that a limit has been reached where errors of different ingredients of the calculation compensate each other or not. For example, passing to MP2 frequencies would shift the harmonic result 1.5 kJ/mol away from experiment (see Supporting Information). Moreover, the estimated uncertainty of our energies is ± 1.4 kJ/mol (section 3.3).

Our isotherm for N$_2$ (313 K) also agrees within the 1 kJ/mol free energy range with those of grand canonical Monte Carlo (GCMC) simulations that use a force field fitted on MP2

Table 7. Comparison of Calculated and Measured Thermodynamic Functions (kJ/mol) for CO/CPO-27-Mg

	ΔH		−TΔS		ΔG	
T (K)	298	318	298	318	298	318
periodic B3LYP+D*, Cart. freq[a,b]	−30.0		33.0		3.0	
this work, "Harm" freq	−38.6[c]		40.5		1.9	
this work, "Anharm" freq	−39.0	−38.9	37.8	40.2	−1.1	1.3
Clausius−Clapeyron/ads. isotherm[d]	−35.4	−35.4[e]	33.4	35.7[e]	−2.0	0.3
VTIR spectroscopy[b]	−29 ± 1	−29[e]	−39 ± 3	−42 ± 3[e]	10	13

[a]Cartesian displacement and harmonic approximation. [b]From ref 12. [c]ΔH(297) = −34.5 kJ/mol, periodic vdW-DF2, Cart. freq.[29] [d]From ref 9. [e]Adsorption enthalpy and entropy are assumed to be temperature-independent in this narrow range of 298−318 K.

cluster calculations,[32] that is, results obtained by an alternative ab initio approach. The perfect agreement of the latter (after scaling with 76.5%, the experimental availability of sites) with experiment again does not mean that a higher precision has been reached, but rather that some error compensation is involved. The GCMC simulations do not account for ZPV energies (2.8 kJ/mol), and the electronic energies used for fitting do not include coupled cluster corrections (4 kJ/mol, Table 3).

3.5.2. Enthalpy, Entropy, and Gibbs Free Energy of Adsorption. Adsorption enthalpies and entropies measured with different experimental techniques for CO and N_2 are compared with thermodynamic functions calculated with various theoretical methods in Tables 7 and 8, respectively.

Table 8. Comparison of Calculated and Measured Thermodynamic Functions (kJ/mol) for N_2/CPO-27-Mg

methods	T (K)	ΔH	−TΔS	ΔG
periodic B3LYP+D + Cart. freq[a]	100	−25.2	12.0	−13.2
this work, "Harm" freq	100	−29.5	11.1	−18.5
this work, "Anharm" freq	100	−29.7	11.7	−18.0
VTIR spectroscopy[a]	100	−21	13.1	−8
this work, "Harm" freq	298	−28.4[b]	33.1	4.7
this work, "Anharm" freq	298	−28.9	31.8	2.9
Clausius−Clapeyron/ads. isotherm[c]	273−292	−23.6		

[a]From ref 12. [b]ΔH(297) = −27.5 kJ/mol, periodic vdW-DF2 + Cart. freq.[29] [c]From ref 68.

For CO, Bloch et al.[9] reported experimental values for both entropies and enthalpies of adsorption, which they obtained from fitting the isotherm data for three different temperatures (298, 308, and 318 K) to a Langmuir model. Applying the Clausius−Clapeyron equation to these isotherm data yielded −35.4 kJ/mol for the adsorption enthalpy.[9] The Gibbs free energy obtained with this enthalpy and the entropy from the fit in ref 9, which is also shown in Table 7, agrees within 1 kJ/mol with our calculated anharmonic Gibbs free energy of adsorption, whereas a deviation of 3.6 kJ/mol is observed for the adsorption enthalpy. The reason is that the fit according to eq 2 may yield a unique K_{BW} value, but there is no unique fitting result for ΔS and ΔH (eqs 1 and 2).

Based on the very good agreement for the Gibbs free energies, we conclude that adsorption enthalpies directly calculated with ab initio methods (eq 4) are more reliable than data obtained with Clausius−Clapeyron calculations from experimental isotherms. For N_2 (Table 8), application of the Clausius−Clapeyron equation also yields adsorption enthalpies that are 5.3 kJ/mol too positive. For this system, experimental

Gibbs free energies are not available from fitting because isotherms have not been measured for high enough pressures/loadings.

The enthalpies derived from VTIR spectroscopy[12] for CO (298 K) and N_2 (100 K) deviate by as much as 9−10 kJ/mol from our anharmonic ab initio results. A similarly large deviation of 10−12 kJ/mol between the anharmonic ab initio and experimental results for the Gibbs free energy tells us that the VTIR results are not trustworthy in this case. VTIR spectroscopy uses a van't Hoff plot and relies on the assumption that the surface concentration is proportional to the absorbance of the species.[11] This may not always be fulfilled, although favorable agreement with calorimetric data has been stated for adsorption in zeolites;[11] at least for one case (N_2/H-ZSM5), there was a direct comparison. Unfortunately, calorimetric measurements have not been reported for the systems under study.

4. CONCLUSIONS

The presented ab initio approach for calculating Gibbs free energies of adsorption, when combined with the Bragg-Williams/Langmuir model and taking into account the experimental site availability, yields adsorption isotherms in close agreement with experiment. The remaining deviations correspond to an error in the Gibbs free energy of about 1 kJ/mol, significantly smaller than the "chemical accuracy" limit of about 4 kJ/mol (≈1 kcal/mol).

The presented approach uses (i) a DFT dispersion method (PBE+D2) to optimize the structure and to calculate *anharmonic frequencies* for vibrational partition functions and (ii) a "hybrid MP2:(PBE+D2)+ΔCCSD(T)" method to determine electronic energies. Standard state-of-the-art approaches rely on *harmonic* frequencies and use *DFT dispersion* methods also to calculate electronic energies. Compared to this standard approach, our hybrid method changes the adsorption energies by 5−10 kJ/mol (about 20%) depending on the functional. The use of anharmonic instead of harmonic frequencies has very little effect on the adsorption enthalpy (0.2−0.5 kJ/mol stronger adsorption), whereas it changes the entropy contribution to the Gibbs free energy ($T\Delta S$) by 1−3 kJ/mol in favor of adsorption. This change of the Gibbs free energy toward stronger adsorption (more negative ΔG) due to anharmonicity is much smaller than the 15−20 kJ/mol found before for small alkanes in H-zeolites (chabazite).[7]

The good agreement of our anharmonic/hybrid results with adsorption isotherms and Gibbs free energies derived from adsorption isotherms makes electronic energies, enthalpies, and entropies obtained with our methodology suitable benchmarks, not only for different DFT dispersion methods (energy) but also for assessing experimental adsorption data such as

enthalpies or entropies derived from VTIR experiments[11,12] or from Clausius−Clapeyron analysis of isotherms.[9,10]

For the adsorption energies, we conclude that the PBE+D2 and vdW-DF2 functionals yield better results (1−5 kJ/mol to small) than the B3LYP+D* functional (5−9 kJ/mol to small). Whereas the Gibbs free energies obtained from Langmuir fits of experimental isotherms agree with our anharmonic/hybrid energy benchmark data within 1 kJ/mol, the deviation is significantly larger (about 5 kJ/mol) for enthalpies and entropy terms obtained via the Clausius−Clapeyron equation from experimental isotherms.

Differently from what has been reported for adsorption of small molecules in zeolites,[11] for the systems studied here, VTIR spectroscopy does not seem to yield reliable results.[12] The reported Gibbs free energy of adsorption is 12−13 kJ/mol larger (more positive) than the value derived from the experimental isotherms. It is also 10−12 kJ/mol larger than our anharmonic/hybrid energy benchmark result. This deviation is largely due to the enthalpy term (9−10 kJ/mol binding is missing), whereas the entropy term shows deviations between 1 and 2 kJ/mol only—within the 3 kJ/mol error bar reported in the VTIR study.

■ ASSOCIATED CONTENT

Ⓢ Supporting Information

The Supporting Information is available free of charge on the ACS Publications website at DOI: 10.1021/jacs.6b08646.

Additional structure figures, additional adsorption isotherms, comparison with previous isotherm calculations, relaxation energies, CCSD(T)−MP2 energy differences, calculation of anharmonic vibrational energies, total electronic energies, and x,y,z coordinates for periodic structures (PDF)

■ AUTHOR INFORMATION

Corresponding Author
*js@chemie.hu-berlin.de
Notes
The authors declare no competing financial interest.

■ ACKNOWLEDGMENTS

■ REFERENCES

(1) Kim, J.; Lin, L. C.; Martin, R. L.; Swisher, J. A.; Haranczyk, M.; Smit, B. *Langmuir* **2012**, *28*, 11914.

(2) Wilmer, C. E.; Leaf, M.; Lee, C. Y.; Farha, O. K.; Hauser, B. G.; Hupp, J. T.; Snurr, R. Q. *Nat. Chem.* **2012**, *4*, 83.

(3) Curtiss, L. A.; Redfern, P. C.; Raghavachari, K. *J. Chem. Phys.* **2005**, *123*, 124107.

(4) Zhao, Y.; Truhlar, D. G. *Acc. Chem. Res.* **2008**, *41*, 157.

(5) Neese, F.; Hansen, A.; Wennmohs, F.; Grimme, S. *Acc. Chem. Res.* **2009**, *42*, 641.

(6) Boese, A. D.; Sauer, J. *Phys. Chem. Chem. Phys.* **2013**, *15*, 16481.

(7) Piccini, G.; Alessio, M.; Sauer, J.; Zhi, Y.; Liu, Y.; Kolvenbach, R.; Jentys, A.; Lercher, J. A. *J. Phys. Chem. C* **2015**, *119*, 6128.

(8) Dietzel, P. D. C.; Blom, R.; Fjellvåg, H. *Eur. J. Inorg. Chem.* **2008**, *2008*, 3624.

(9) Bloch, E. D.; Hudson, M. R.; Mason, J. A.; Chavan, S.; Crocellà, V.; Howe, J. D.; Lee, K.; Dzubak, A. L.; Queen, W. L.; Zadrozny, J. M.; Geier, S. J.; Lin, L.-C.; Gagliardi, L.; Smit, B.; Neaton, J. B.; Bordiga, S.; Brown, C. M.; Long, J. R. *J. Am. Chem. Soc.* **2014**, *136*, 10752.

(10) Mason, J. A.; Sumida, K.; Herm, Z. R.; Krishna, R.; Long, J. R. *Energy Environ. Sci.* **2011**, *4*, 3030.

(11) Garrone, E.; Otero Arean, C. *Chem. Soc. Rev.* **2005**, *34*, 846.

(12) Valenzano, L.; Civalleri, B.; Chavan, S.; Palomino, G. T.; Areán, C. O.; Bordiga, S. *J. Phys. Chem. C* **2010**, *114*, 11185.

(13) Odoh, S. O.; Cramer, C. J.; Truhlar, D. G.; Gagliardi, L. *Chem. Rev.* **2015**, *115*, 6051.

(14) Hobza, P.; Sauer, J.; Morgeneyer, C.; Hurych, J.; Zahradník, R. *J. Phys. Chem.* **1981**, *85*, 4061.

(15) Tuma, C.; Sauer, J. *Angew. Chem., Int. Ed.* **2005**, *44*, 4769.

(16) De Moor, B. A.; Reyniers, M. F.; Marin, G. B. *Phys. Chem. Chem. Phys.* **2009**, *11*, 2939.

(17) Van Speybroeck, V.; Van der Mynsbrugge, J.; Vandichel, M.; Hemelsoet, K.; Lesthaeghe, D.; Ghysels, A.; Marin, G. B.; Waroquier, M. *J. Am. Chem. Soc.* **2011**, *133*, 888.

(18) De Moor, B. A.; Ghysels, A.; Reyniers, M. F.; Van Speybroeck, V.; Waroquier, M.; Marin, G. B. *J. Chem. Theory Comput.* **2011**, *7*, 1090.

(19) Antony, A.; Hakanoglu, C.; Asthagiri, A.; Weaver, J. F. *J. Chem. Phys.* **2012**, *136*, 054702.

(20) Shang, J.; Li, G.; Singh, R.; Xiao, P.; Danaci, D.; Liu, J. Z.; Webley, P. A. *J. Chem. Phys.* **2014**, *140*, 084705.

(21) Tuma, C.; Sauer, J. *Chem. Phys. Lett.* **2004**, *387*, 388.

(22) Tuma, C.; Sauer, J. *Phys. Chem. Chem. Phys.* **2006**, *8*, 3955.

(23) Piccini, G.; Sauer, J. *J. Chem. Theory Comput.* **2013**, *9*, 5038.

(24) Piccini, G.; Sauer, J. *J. Chem. Theory Comput.* **2014**, *10*, 2479.

(25) Piccini, G.; Alessio, M.; Sauer, J. *Angew. Chem., Int. Ed.* **2016**, *55*, 5235.

(26) Alexopoulos, K.; Lee, M.-S.; Liu, Y.; Zhi, Y.; Liu, Y.; Reyniers, M.-F.; Marin, G. B.; Glezakou, V.-A.; Rousseau, R.; Lercher, J. A. *J. Phys. Chem. C* **2016**, *120*, 7172.

(27) Valenzano, L.; Civalleri, B.; Sillar, K.; Sauer, J. *J. Phys. Chem. C* **2011**, *115*, 21777.

(28) Lee, K.; Isley, W. C.; Dzubak, A. L.; Verma, P.; Stoneburner, S. J.; Lin, L.-C.; Howe, J. D.; Bloch, E. D.; Reed, D. A.; Hudson, M. R.; Brown, C. M.; Long, J. R.; Neaton, J. B.; Smit, B.; Cramer, C. J.; Truhlar, D. G.; Gagliardi, L. *J. Am. Chem. Soc.* **2014**, *136*, 698.

(29) Lee, K.; Howe, J. D.; Lin, L.-C.; Smit, B.; Neaton, J. B. *Chem. Mater.* **2015**, *27*, 668.

(30) Rosi, N. L.; Kim, J.; Eddaoudi, M.; Chen, B.; O'Keeffe, M.; Yaghi, O. M. *J. Am. Chem. Soc.* **2005**, *127*, 1504.

(31) Wales, D. J. *Energy Landscapes: Applications to Clusters, Biomolecules and Glasses*; Cambridge University Press: Cambridge, U.K., 2003.

(32) Dzubak, A. L.; Lin, L.-C.; Kim, J.; Swisher, J. A.; Poloni, R.; Maximoff, S. N.; Smit, B.; Gagliardi, L. *Nat. Chem.* **2012**, *4*, 810.

(33) Chen, L.; Morrison, C. A.; Düren, T. *J. Phys. Chem. C* **2012**, *116*, 18899.

(34) Bučko, T.; Benco, L.; Hafner, J.; Ángyán, J. G. *J. Catal.* **2007**, *250*, 171.

(35) Jiang, T.; Göltl, F.; Bulo, R. E.; Sautet, P. *ACS Catal.* **2014**, *4*, 2351.

(36) Sillar, K.; Hofmann, A.; Sauer, J. *J. Am. Chem. Soc.* **2009**, *131*, 4143.

(37) Sillar, K.; Sauer, J. *J. Am. Chem. Soc.* **2012**, *134*, 18354.

(38) Steele, W. A. *The Interaction of Gases with Solid Surfaces*; Pergamon Press: Oxford, U.K., 1974.

(39) Perdew, J. P.; Burke, K.; Ernzerhof, M. *Phys. Rev. Lett.* **1996**, *77*, 3865.

(40) Perdew, J. P.; Burke, K.; Ernzerhof, M. *Phys. Rev. Lett.* **1997**, *78*, 1396.

(41) Grimme, S. *J. Comput. Chem.* **2006**, *27*, 1787.

(42) Kresse, G.; Furthmüller, J. *Comput. Mater. Sci.* **1996**, *6*, 15.

(43) Kresse, G.; Furthmüller, J. *Phys. Rev. B: Condens. Matter Mater. Phys.* **1996**, *54*, 11169.

(44) Kerber, T.; Sierka, M.; Sauer, J. *J. Comput. Chem.* **2008**, *29*, 2088.

(45) Tosoni, S.; Sauer, J. *Phys. Chem. Chem. Phys.* **2010**, *12*, 14330.

(46) Hättig, C.; Weigend, F. *J. Chem. Phys.* **2000**, *113*, 5154.

(47) *TURBOMOLE* V6.5, 2013; a development of University of Karlsruhe and Forschungszentrum Karlsruhe GmbH, 1989−2007, TURBOMOLE GmbH, since 2007; available from http://www.turbomole.com.

(48) Boys, S. F.; Bernardi, F. *Mol. Phys.* **1970**, *19*, 553.

(49) Dunning, T. H. *J. Chem. Phys.* **1989**, *90*, 1007.

(50) Kendall, R. A.; Dunning, T. H.; Harrison, R. J. *J. Chem. Phys.* **1992**, *96*, 6796.

(51) Halkier, A.; Helgaker, T.; Jorgensen, P.; Klopper, W.; Koch, H.; Olsen, J.; Wilson, A. K. *Chem. Phys. Lett.* **1998**, *286*, 243.

(52) Jensen, F. *Theor. Chem. Acc.* **2005**, *113*, 267.

(53) Helgaker, T.; Klopper, W.; Koch, H.; Noga, J. *J. Chem. Phys.* **1997**, *106*, 9639.

(54) Cramer, C. J. *Essentials of Computational Chemistry: Theories and Models*; Wiley: New York, 2004.

(55) Tait, S. L.; Dohnalek, Z.; Campbell, C. T.; Kay, B. D. *J. Chem. Phys.* **2005**, *122*, 164708.

(56) Campbell, C. T.; Sprowl, L. H.; Árnadóttir, L. *J. Phys. Chem. C* **2016**, *120*, 10283.

(57) Sprowl, L. H.; Campbell, C. T.; Árnadóttir, L. *J. Phys. Chem. C* **2016**, *120*, 9719.

(58) Njegic, B.; Gordon, M. S. *J. Chem. Phys.* **2006**, *125*, 224102.

(59) McQuarrie, D. A. *Statistical Mechanics*; Harper Collins Publishers: New York, 1976; Chapter 3.

(60) Zhou, W.; Wu, H.; Yildirim, T. *J. Am. Chem. Soc.* **2008**, *130*, 15268.

(61) Xiao, D. J.; Bloch, E. D.; Mason, J. A.; Queen, W. L.; Hudson, M. R.; Planas, N.; Borycz, J.; Dzubak, A. L.; Verma, P.; Lee, K.; Bonino, F.; Crocella, V.; Yano, J.; Bordiga, S.; Truhlar, D. G.; Gagliardi, L.; Brown, C. M.; Long, J. R. *Nat. Chem.* **2014**, *6*, 590.

(62) Queen, W. L.; Brown, C. M.; Britt, D. K.; Zajdel, P.; Hudson, M. R.; Yaghi, O. M. *J. Phys. Chem. C* **2011**, *115*, 24915.

(63) Caskey, S. R.; Wong-Foy, A. G.; Matzger, A. J. *J. Am. Chem. Soc.* **2008**, *130*, 10870.

(64) Sauer, J.; Ugliengo, P.; Garrone, E.; Saunders, V. R. *Chem. Rev.* **1994**, *94*, 2095.

(65) Nijem, N.; Canepa, P.; Kong, L.; Wu, H.; Li, J.; Thonhauser, T.; Chabal, Y. J. *J. Phys.: Condens. Matter* **2012**, *24*, 424203.

(66) Schwabe, T.; Grimme, S. *J. Phys. Chem. A* **2009**, *113*, 3005.

(67) Sherrill, C. D.; Takatani, T.; Hohenstein, E. G. *J. Phys. Chem. A* **2009**, *113*, 10146.

(68) Perry, J. J.; Teich-McGoldrick, S. L.; Meek, S. T.; Greathouse, J. A.; Haranczyk, M.; Allendorf, M. D. *J. Phys. Chem. C* **2014**, *118*, 11685.